IMPACT OF DIFFERENT VEHICLE MODELS ON THREAT ASSESSMENT IN CRITICAL CURVE SITUATIONS

Mohammad Ali
Volvo Car Corporation
Jonas Sjöberg
Chalmers University of Technology
Sweden
Paper Number 09-0076

ABSTRACT

Curve speed warning systems (CSW) utilize information about the road and warn drivers if they are about to enter a curve too fast. Recent research shows that CSW is successful in warning for upcoming curves. However no statistically significant change in driver behaviour due to CSW has been shown. In addition, a common requirement cited by drivers is that the amount of false alarms needs to be reduced.

This paper evaluates how the level of detail in the modelled vehicle dynamics influences the threat assessment in a situation with an oncoming curve. The point mass model that is commonly used by CSW is compared with more detailed models. Maximum velocity the vehicle can have while still following a curve is investigated and compared for the point mass model, the single track model and the double track model. It is shown that as the level of detail in the modelled dynamics increase, the maximum velocity profile is significantly reduced. This implies that in order to make a reliable threat assessment that can reduce the amount of false alarms and even be used as a base for an autonomous intervention, a more complex vehicle model than the point mass model is required.

INTRODUCTION

The number of fatalities in vehicles leaving the road due to loss of control has been greatly reduced since car manufacturers started to equip vehicles with electronic stability systems, [1]. Despite this, unintended roadway departures still account for the highest share of traffic related fatalities, [2][3]. Roadway departures are thus still a highly significant problem.

Currently a new type of active safety systems that also addresses roadway departures is emerging. Curve speed warning systems (CSW) utilize sensor data about the road and warn drivers if they are about to enter a curve too fast. In [3], it is shown that CSW is successful in warning for upcoming curves. CSW might therefore give a significant contribution to further reduction of roadway departures, provided that drivers take the warnings seriously.

However, in the study presented in [3], no statistically significant change in driver behaviour due to CSW could be shown. Even though the concept of CSW was generally thought to increase safety, a common requirement cited by drivers is that the amount of false alarms needs to be reduced. In fact, drivers often commented that when they received a CSW alert, they would make their own evaluation of the situation rather than simply slowing down in response to the alert.

Drivers only experience the system through its interface and it is therefore crucial that false alerts are avoided so that drivers are confident with the system. How to define a false alert can of course be disputed, however alerts which common drivers consider as unnecessary will contribute negatively to their confidence in the system.

In this paper we focus on the threat assessment part of CSW i.e. the part where it is evaluated whether an alert or intervention is required. Current CSW systems attempt to keep drivers within the range of lateral accelerations associated with normal curve taking [3]. In general it can be stated that the threat assessment related with such an approach is suitable for issuing early warnings or calculating reference velocity in curves for e.g. an adaptive cruise control. The starting point of this work is however that drivers need to see a clear connection between an alert from the system and an actual threat in order for the system to gain credibility. In fact, the long term aim is to have a threat assessment that is reliable enough to motivate an intervention rather than just alerting the driver.

In particular, the purpose of this paper is to evaluate how the level of detail in the modelled vehicle dynamics influences the threat assessment in a situation with an oncoming curve. The point mass model that is used by the threat assessment of CSW (see e.g. [3]) is here compared with other, well established vehicle models that are more detailed. The vehicle is modelled using a point mass model, a single track model and a four wheel model. As comparison measure, the maximum

velocity the vehicle can have while still following a particular curve is investigated and compared for the different models. Even though the comparison is quite simple, it shows that the level of detail in the modelled dynamics has a significant impact on the result.

This implies that in order to make a reliable threat assessment that can reduce the amount of false alarms and even be used as a base for an autonomous intervention, a more complex vehicle model than the point mass model is required.

SIMULATION STRATEGY

In this section, the chosen approach for calculating the maximum velocity profile is explained using the point mass vehicle model as an example. In order to compare the different vehicle models, a scenario where a vehicle approaches a specific curve is considered. The curve is represented as a clothoid which means that the curvature increases linearly along the travelled path and can be expressed

$$c(s) = c_0 + c_1 s \quad \textbf{(1)}$$

where c_0 is the curvature at the starting point, c_1 the increase rate of the curvature along the curve and s is the travelled distance along the curve. The construction of real roads corresponds well with equation (1), [4][5]. Clothoids are often used as transitions between straight road segments and segments with constant curvature. In particular, the curve used in all simulations in this paper is a 120m long clothoid that has a radius of 50m at the apex i.e. the end of the clothoid. This curve is quite short and typically suitable as a transition curve followed by a segment with constant curvature on a road with 50 km/h as posted velocity [5].

For a point mass model, the maximum velocity profile through the curve is easily obtained using the principles described in [6]. The equations of motion for a point mass can be stated

$$m\ddot{s} = F_x$$

$$m\dot{s}^2 = \frac{F_y}{c(s)} \quad \textbf{(2)}$$

with m as the vehicles mass, F_x the force in the tangential direction of the path and F_y as the force normal to the direction of travel.

A common assumption regarding available friction force is that it is limited by a friction ellipse [7]. In its simplest form the friction ellipse can be expressed as a circle according to

$$F_x^2 + F_y^2 \le (\mu F_z)^2 \quad \textbf{(3)}$$

where μ is the friction coefficient and F_z is the normal load. Since this is a comparative study, the friction coefficient will be given the same value μ=1 in all simulations which corresponds to assuming that the vehicle travels on dry asphalt.

With F_x and F_y as control inputs, assuming controllability conditions to be fulfilled and the dynamics to be well defined, it is stated in [6] that for the vehicle to exactly follow the path in minimum time, it has been formally proven that the following control law holds

$$F_y = mc\dot{s}^2$$

$$F_x = \pm\sqrt{(\mu F_z)^2 - F_y^2} \quad \textbf{(4)}$$

The control law has been reformulated to fit the notation of this paper. An interpretation of the control law is that as much lateral force as needed to follow the reference curvature should be utilized and the rest of the available force should be used for either full acceleration or full deceleration.

By combining (3) and (2), it can be derived that there exists a critical velocity for which a vehicle can no longer follow the specified curvature

$$\dot{s}_{critical} = \sqrt{\frac{\mu F_z c}{m}} \quad \textbf{(5)}$$

which is the maximum allowable velocity at each point of the path [6]. For the considered curve, the curvature has only one minimum at the end of the clothoid. As a consequence of (5), the optimal velocity profile then also has a minimum at the same point. By setting the critical velocity at the apex as boundary condition and applying the control law (4), the optimal velocity profile can be obtained by starting a simulation at the end of the clothoid where the vehicle travels in the reversed direction.

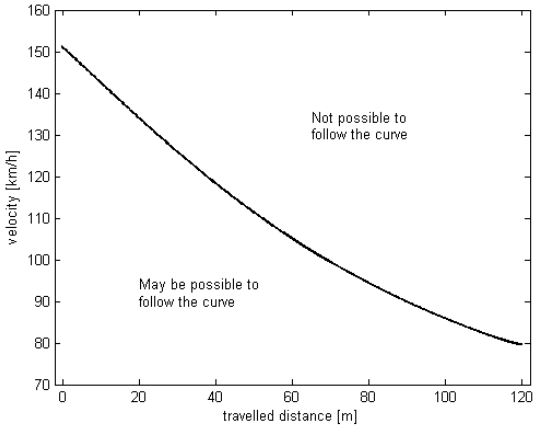

Figure 1. Maximum velocity profile computed using a point mass model.

The result of such a simulation can be seen in Figure 1. The computed velocity profile implies that an optimal driver can enter the curve with a velocity of about 150 km/h and pass the end of the clothoid in about 80 km/h.

Principle of optimality

When the level of detail in the modelled vehicle dynamics is increased it is not straightforward to reverse the direction of motion without first taking care of the inverted dynamics. The vehicle's behaviour during acceleration will be different from the behaviour during deceleration. Consequently the method used above for the point mass is not used here to obtain the optimal velocity profile when more detailed models are considered. Instead the principle of optimality is used which can be stated:

"An optimal policy has the property that whatever the previous state and decision (i.e. control), the remaining decision must constitute an optimal policy with regard to the state resulting from the previous decision." [8]

In other words, the optimal velocity profile can be divided into smaller segments which are themselves optimal. If one can find the optimal solution for the small segments, one can put them together to get the optimal solution for the whole path [8].

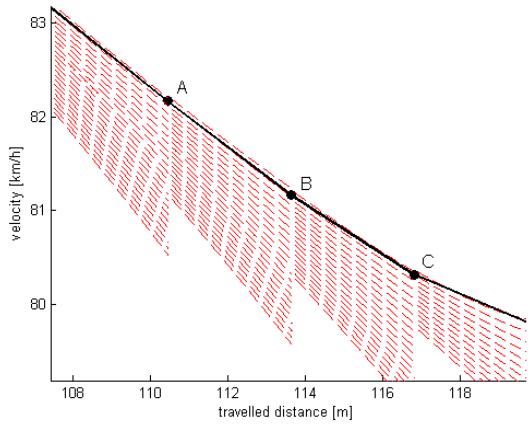

Figure 2. The principle of optimality is used to obtain the optimal velocity profile. The black solid line represents the optimal profile while the red dashed lines represent simulations conducted in order to find the maximum velocity for each segment.

The following bullets together with Figure 2 explain how the principle of optimality is utilized in this study:

- The curve is uniformly divided into several small segments. In Figure 2 this is illustrated by the dividing points A, B and C.
- The optimal velocity at the point C in Figure 2 is assumed to be known and denoted v_c.
- A simulation of the vehicle's motion between the points B and C is conducted where the lateral force needed in order to follow the curve is applied and the rest of the available force is utilized to brake in accordance with the control law (4).
- The vehicle's initial velocity at point B is gradually increased with a predefined resolution as the simulation is iteratively repeated.
- When available brake force is no longer sufficient to reduce the vehicle's velocity below v_c, at point C, the iterations stop.
- The highest velocity the vehicle can have at point B while still reaching point C without exceeding v_c, is then considered to be v_b.
- Once v_b has been acquired, the procedure can be repeated between the points A and B to obtain v_a and analogously for the remaining segments until solutions has been acquired for the whole curve.
- The points A, B and C was here used to give an illustration of the procedure, in reality the procedure is initiated at the end of the clothoid and the maximum velocity at that point is calculated using (5).

The optimal velocity obtained using the principle of optimality is of course an approximation, since the set of possible solutions as well as the curve is discretized. As the resolution is increased, the accuracy of the obtained solution will however improve and if infinite resolution could be achieved, the difference from the true optimum would tend to zero.

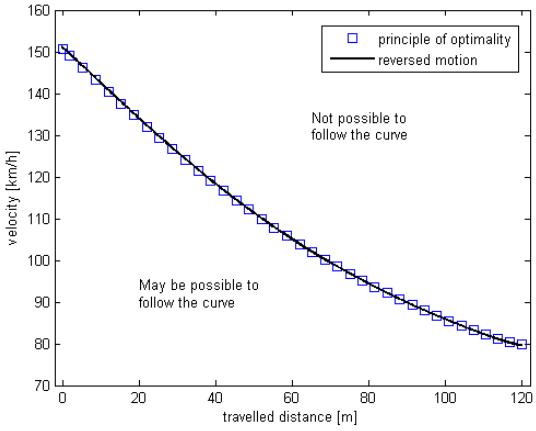

Figure 3. Time optimal velocity profile obtained through reversing the vehicles motion is compared with the solution acquired with the principle of optimality.

In Figure 3, a validation of the chosen resolution is made by comparing the optimal path of a point mass computed by reversing the vehicle's motion and the one computed using the principle of optimality. Even though the solutions are not identical, the difference is satisfactorily small. The principle of optimality will therefore be used in the following sections to obtain optimal velocity profiles for more detailed vehicle models.

SINGLE TRACK VEHICLE MODEL

In a point mass representation of the vehicle, the wheelbase and track width are collapsed to zero, hence all forces are applied on the centre of mass. In this section, a single track model is considered, which means that the car's length and orientation is also taken into account. Applied forces are distributed between the front and rear axle and might therefore also cause the vehicle to rotate around its own axis rather than just moving the mass centre. Without loss of generality each axle is here considered as a tire and with notation defined in Figure 4 the equations of motion can then be expressed, [9]

$$\dot{\psi} = \frac{1}{J_z}(F_{fy} l_f - F_{ry} l_r)$$

$$\dot{v}_x = \frac{1}{m}(F_{fx} + F_{rx}) + v_y \dot{\psi}$$

$$\dot{v}_y = \frac{1}{m}(F_{fy} + F_{ry}) - v_x \dot{\psi} \qquad \textbf{(6)}$$

Note however that the forces in (6), are denoted F and expressed in the vehicle frame which is different from the forces denoted f in Figure 4 which are expressed in the tire's coordinate system. The forces can easily be expressed in the vehicle frame by feeding the forces in Figure 4 through the following coordinate transformation

$$F_{fx} = f_{fx}\cos(\delta) - f_{fy}\sin(\delta)$$

$$F_{fy} = f_{fx}\sin(\delta) + f_{fy}\cos(\delta)$$

$$F_{rx} = f_{rx}$$

$$F_{ry} = f_{ry} \qquad \textbf{(7)}$$

The acceleration limits are in this case given by two friction ellipses, one at each tire. An illustration is given in Figure 5, it can be seen that combinations of the forces at each tire can achieve a total force anywhere in the dashed ellipse which represents the total friction limit.

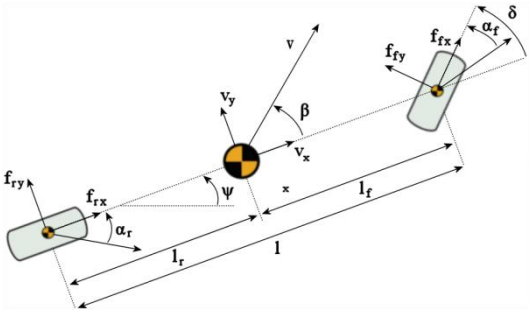

Figure 4. Notation for the single track model.

In conventional vehicles, lateral force is however in general generated by turning the front wheel and brake force by applying braking torque on the wheels. By turning the front wheel, the lateral force at the front can thus be directly controlled while the lateral force at the rear is completely determined by the state of the vehicle and only indirectly influenced by the front wheel angle. In addition, a driver can only control brake torque through a brake pedal which distributes brake torque between the front and rear axle with a fix ratio. Under the assumption that no active systems like e.g. the antilock brake system intervenes, one can therefore say that the torque distribution and hence longitudinal force distribution between the front and back wheel is fixed. These limitations imply that arbitrary combinations of the forces at the front and the rear wheel may not be achieved by a driver and it is not certain that the force applied on the vehicle can always be anywhere in the friction ellipse.

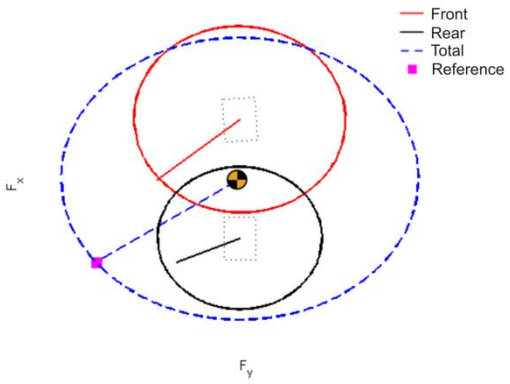

Figure 5. Tire forces with constraints. The lines represent forces while the ellipses surrounding them are bounding constraints.

In order to adopt a control strategy corresponding to (4), a cascade control with an inner control loop that delivers the required force is introduced. The inner control loop is required since the mapping from applied wheel angle and brake torque to acquired force is dynamic. The adopted control strategy is illustrated by the block diagram in Figure 6 where

- The block **C1**, compares the vehicle's state with the desired path and decides which lateral and longitudinal forces that needs to be applied on the vehicle in the same fashion as in (4). In Figure 5, the output of **C1** i.e. the required force is represented by the square that is located at the limit of the dashed ellipse.
- The block **C2**, which is much faster than **C1**, compares the generated force i.e. the dashed line in Figure 5, with the required force and decides which wheel angle and brake torque that is required in order to achieve the force demanded by **C1**.
- The wheel torque, which is one of the outputs of **C2** is a "total" torque, T_{tot}. The torque, T_{tot} is distributed between the front and back wheel according to

$$T_f = 0.7T_{tot} \qquad T_r = 0.3T_{tot} \qquad \textbf{(8)}$$

The larger portion of the torque is applied at the front since the normal load is greater there for the vehicle considered in this study.

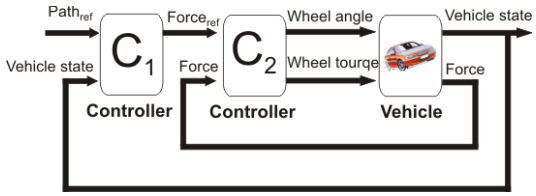

Figure 6. Block diagram describing the control strategy.

In addition to introducing the cascade control we also need to model the mapping from wheel angle and wheel torque to the forces acting on the vehicle. Two different approaches is tested here, one linear tire model (with saturation) and one nonlinear tire model. The tire models are explained in the following subsections.

Linear Tires

The longitudinal force at each tire is calculated as a function of the longitudinal slip. In order to keep track of the longitudinal slip, the rotational velocity is introduced as an additional state for each tire. The state model is therefore extended with

$$\dot{\omega}_i = (T_i - f_{xi})\frac{1}{J_\omega} \qquad i=f,r \qquad \textbf{(9)}$$

where J_ω denotes wheel inertia, T_i denotes wheel torque, ω_i denotes rotational velocity of the wheel and f_{xi} denotes longitudinal force expressed in the tires coordinate system. Given the rotational velocity at each wheel, one can calculate the longitudinal slip κ as

$$\kappa_i = -(1 - \frac{\omega_i r}{v_x}) \qquad i=f,r \qquad \textbf{(10)}$$

where r denotes the effective wheel radius [10].

A simple way of representing the relation between the longitudinal slip and longitudinal force at a wheel is by the linear relation

$$f_{xi} = K_{xi}\kappa_i \qquad i=f,r \qquad \textbf{(11)}$$

with K_{xi} as longitudinal stiffness.

Also the lateral force can be approximated using a linear relation. The mapping from lateral slip to lateral force is then

$$f_{yi} = K_{yi}\alpha_i \qquad i=f,r \qquad \textbf{(12)}$$

with K_{yi} as cornering stiffness and α_i as the tire slip angle as defined in Figure 4, this linear representation is commonly used in electronic stability systems, see e.g. [11] and [12].

For the front wheel the slip angle is easily derived by considering Figure 4 as

$$\alpha_f = \frac{v_y + l_f\dot{\psi}}{v_x} - \delta \qquad \textbf{(13)}$$

and for the rear wheel it is calculated as

$$\alpha_r = \frac{v_y - l_r\dot{\psi}}{v_x} \qquad \textbf{(14)}$$

The stiffness parameters K_{xi} and K_{yi} are acquired by linearizing the tire characteristics around κ_i=0 and α_i=0, [7].

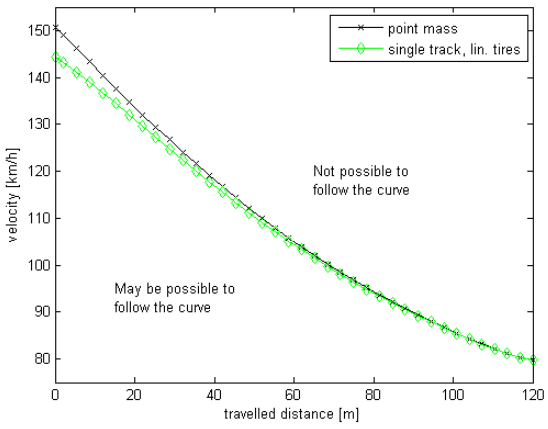

Figure 7. Time optimal velocity profile.

Figure 7 shows a comparison between the result obtained with the point mass model and the result obtained using the single track model with linear tires. Since the same boundary value is used for both models and most of the available force is utilized laterally to follow the path, the velocity

profiles are quite similar to each other at the end of the clothoid. However, earlier in the curve when more of the available force can be used longitudinally the difference is higher.

Nonlinear Tires

The primary external influence on the vehicle's behaviour is provided by the tire forces and it is therefore important to have a realistic nonlinear tire model when investigating vehicle motion near the limits of manoeuvring capability, [10].

In Figure 8, lateral force characteristics are illustrated for different values of the friction coefficient. It can be seen that for small slip angles, a linear approximation of the tire works well. In normal driving conditions this is where the tire operates and the linear approximation is therefore useful. As the operating point gets closer to the limit of adhesion, the nonlinearity however becomes more evident and eventually, the tire force saturates and then starts to decrease.

Also for the longitudinal force, the nonlinearity becomes more evident as the slip value is increased. This can be seen in Figure 9 which shows longitudinal force characteristics.

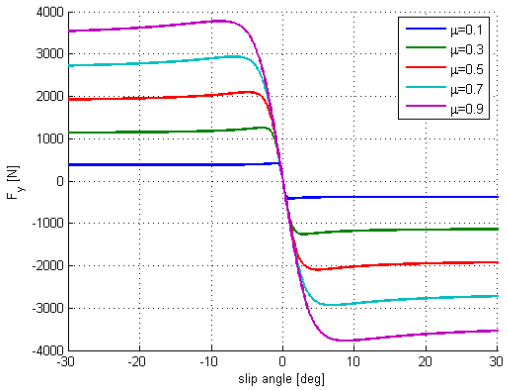

Figure 8. Lateral tire force.

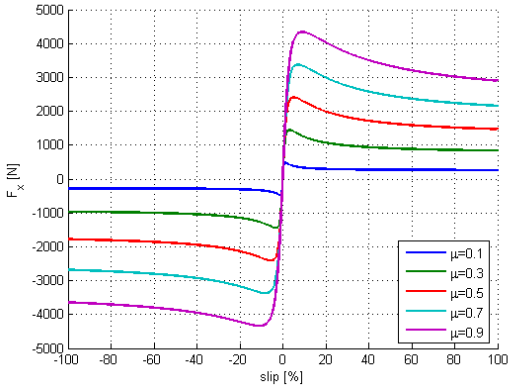

Figure 9. Longitudinal tire force.

There is a strong coupling between the longitudinal and lateral tire force. The illustrations in Figure 8 and Figure 9 are only valid in either pure cornering or pure braking. If both lateral and longitudinal force is produced at the same time, they will influence each other. Figure 10 shows lateral force as a function of lateral slip for different values of the longitudinal slip. It can be seen that if longitudinal force is utilized, the acquired lateral force is reduced. Figure 11 also shows that the analogue relation holds for longitudinal force.

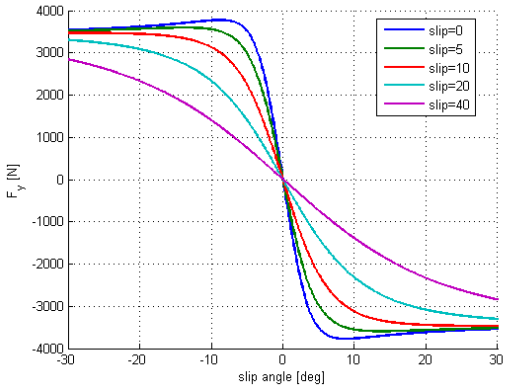

Figure 10. Lateral tire force during combined slip for μ=0.9.

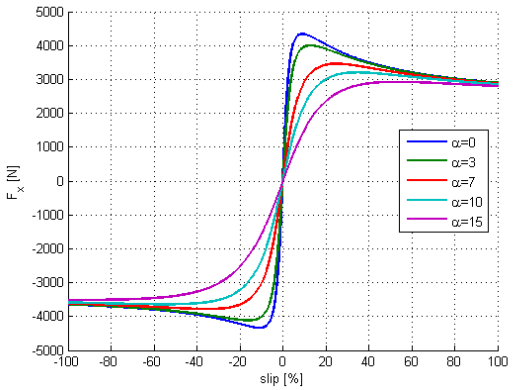

Figure 11. Longitudinal tire force during combined slip for μ=0.9.

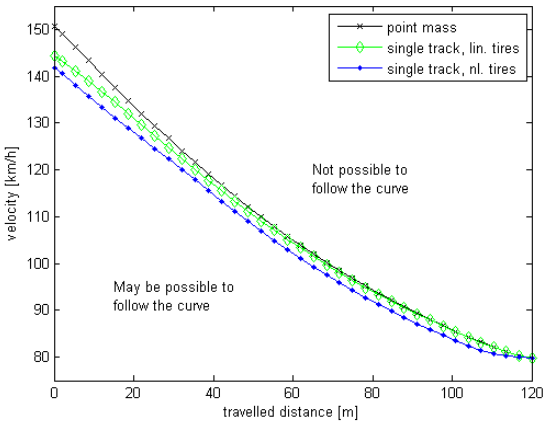

Figure 12. Time optimal velocity profile

One common way to model tire characteristics is by the empirical magic tire formula. The formula is a curve fitting which takes into account the nonlinear nature of a tire in a good way. The coupling between longitudinal and lateral force can be taken into consideration using the combined slip form of the formula

$$f_x = f_{x0}(\kappa, F_z) G_{x\alpha}(\alpha, \kappa, F_z)$$

$$f_y = f_{y0}(\alpha, F_z) G_{x\kappa}(\alpha, \kappa, F_z) \quad \textbf{(15)}$$

where f_x and f_y are lateral and longitudinal forces, f_{x0} and f_{y0} are the forces calculated for pure braking or cornering and $G_{x\kappa}$ and $G_{x\alpha}$ are weight factors that take care of the combined slip effect. A comprehensive treatment of the magic tire formula is given in [13].

Figure 12 shows the obtained profile when the magic tire formula is used to model the tires. The same boundary condition is used in this case as for the previous models. It can be seen that there is a noticeable difference in slope between the profiles for the linear and the nonlinear tire model in the end of the clothoid. The difference is however less evident earlier in the curve. This is due to that in the case with the nonlinear tire model, a higher share of the available force is used in the lateral direction. As a consequence of the coupling between longitudinal and lateral force, the braking has to "stop" earlier along the path so that enough lateral force to follow the curve can be produced.

Longitudinal Load Transfer

In Figure 5, the friction ellipse constraining the tire force at the front wheel is larger than the ellipse at the rear. This is due to that the modelled vehicle, as mentioned earlier, has a larger portion of its weight in the front. Available and acquired tire force is thus dependant on the normal load on the tire.

If the height of the vehicle is taken into consideration, the normal load at each tire is no longer considered to be constant. When longitudinal force is applied, a moment around the vehicle's y-axis is generated. Depending on whether the vehicle is accelerating or decelerating, this moment is balanced by an increase in normal load at either the front or the rear tire. The longitudinal load transfer can be calculated

$$\Delta F_z = \frac{(F_{fx} + F_{rx})h}{l} \quad \textbf{(16)}$$

with h as the height of the vehicle's mass centre. A derivation of equation (16) is provided in [14].

Obviously since the normal load has a direct influence on acquired force, it affects the manoeuvrability of the vehicle. It is therefore interesting to evaluate what effect the longitudinal load transfer has on the optimal velocity profile. In Figure 13, the velocity profile for a single track model with nonlinear tires and longitudinal load transfer has been added. Figure 13 reveals that the load transfer has a slightly positive influence on the time optimal velocity profile. When brake force is applied, the normal load at the front tire is increased. Since applied brake torque is in our case higher at the front, this results in a higher total longitudinal force. However as the vehicle moves further along the curve and the curvature increases, the difference disappears since the limiting factor becomes available lateral force.

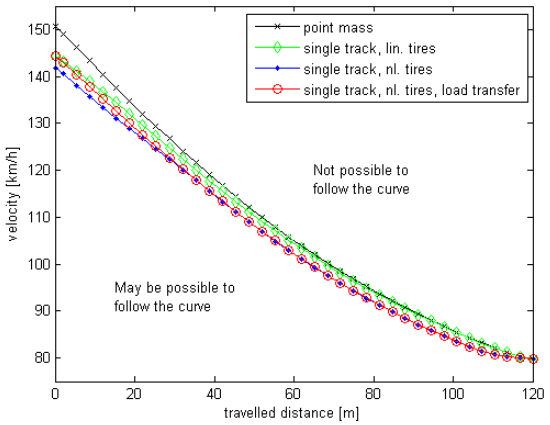

Figure 13. Time optimal velocity profile.

DOUBLE TRACK VEHICLE MODEL

In this section, we also take into account that the vehicle has a width. The equations of motion are then

$$\dot{\psi} = \frac{1}{J_z}\left[(-F_{1x} + F_{2x} - F_{3x} + F_{4x})\frac{w}{2}\right.$$

$$\left. + (F_{1y} + F_{2x})l_f - (F_{3y} + F_{4y})l_r \right]$$

$$\dot{v}_x = \frac{1}{m}(F_{1x} + F_{2x} + F_{3x} + F_{4x}) + v_y\dot{\psi}$$

$$\dot{v}_y = \frac{1}{m}(F_{1y} + F_{2y} + F_{3y} + F_{4y}) - v_x\dot{\psi}$$

$$\dot{\omega}_i = (T_i - f_{ix}r)\frac{1}{J_\omega} \qquad i = 1,2,3,4 \quad \textbf{(17)}$$

where J_ω is the wheel inertia and the rest of the notation is defined in Figure 14. As above, forces are denoted f when expressed in the tires coordinate system and F in the vehicle frame.

When the vehicle's height was taken into consideration for the single track model, we saw that the vehicle's vertical load varies when longitudinal force is applied. Similarly, taking the

vehicle's width into account reveals a lateral load transfer. The lateral load transfer can be calculated

$$\Delta F_{fz_{lat}} = \frac{\dot{\psi} v_x m}{w}\left[\frac{h_{rf} l_r}{l} + R_{sf}(h - h_{rc})\right]$$

$$\Delta F_{rz_{lat}} = \frac{\dot{\psi} v_x m}{w}\left[\frac{h_{rr} l_f}{l} + R_{sr}(h - h_{rc})\right] \quad \textbf{(18)}$$

where R_{sf} and R_{sr} is the roll stiffness distribution at the front and rear axles and the rest of the notation is defined in Figure 14.

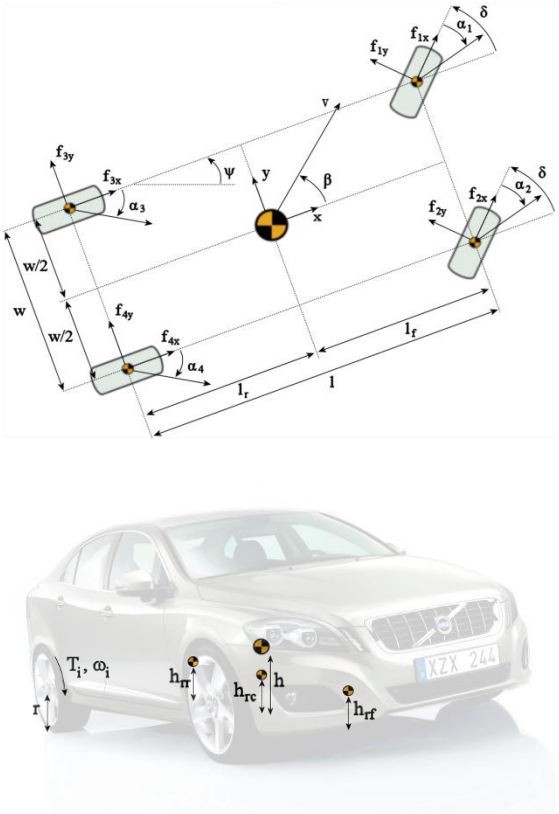

Figure 14. Notation for the double track model.

The equations presented earlier to calculate e.g. the slip quantities for the single track model can easily be extended to fit the double track model. An extensive treatment of the double track model is however omitted here and the reader is referred to [14] where a complete derivation is provided together with the assumptions it is based on.

With different vertical load at each tire, the forces generated at the contact patch of the tires will also be different even if they have the same slip values. The longitudinal forces will then contribute to the yaw moment imposed on the vehicle, especially in cornering when the lateral load transfer is large. The additional yaw moment might cause instability in the vehicle's behaviour if it is too large and it is therefore worth examining the impact of this phenomenon on the maximum velocity profile.

In Figure 15, the optimal velocity profile for the double track model has been added. The nonlinear tire model with both longitudinal and lateral load transfer has been used. It is clear that the velocity profile is lower for the double track model. In addition to the yaw moment caused by the difference in longitudinal forces, uneven distribution of the vertical load between the right and the left side also reduces the total amount of lateral force available. A lower velocity is therefore required at each point of the path in order for the lateral force to be sufficient to keep the vehicle following the curve.

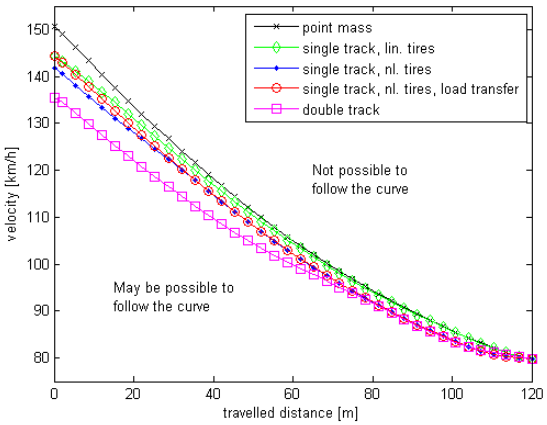

Figure 15. Time optimal velocity profile.

DISCUSSION & FUTURE WORK

In this paper, maximum velocity profiles for a vehicle travelling through a specific curve were computed using a set of well known vehicle models. It was found that the resulting velocity profile differs significantly between the simplest and the most detailed model. This is especially remarkable since the curve considered in this study is only 120m long and suited for 50km/h as posted velocity. The curve is thus relatively short and greater differences can be expected for longer curves.

Information about the maximum velocity a vehicle can have while still following the road can be used in an active safety system to either warn drivers or assist them by issuing autonomous interventions. If the car travels faster than the maximum velocity at any point along the curve, it is impossible for the vehicle to stay on the road and an autonomous intervention can then be motivated. This approach is conservative and guarantees that false alerts or interventions are never issued. As can be seen by the result, the acquired thresholds however becomes very high and in practice such a conservative system will seldom intervene.

Drivers are however never completely optimal, hence a vehicle travelling slower than the computed maximum velocity is not necessarily

safe. In CSW the issue of high thresholds is worked around by introducing a safety factor which basically shifts the velocity profile downwards. The problem with that approach is that, the mapping between the velocity profile and an actual threat is then lost. This is acceptable for a system that warns for upcoming curves but cannot be used as a base for autonomous interventions.

The velocity profiles computed in this paper only considers how fast it is possible for a vehicle to travel through the curve and does not say anything about how difficult it is. A common assumption is that it is difficult for normal drivers to manoeuvre a vehicle operating in the nonlinear region of the tires [11]. This assumption is the base of current state of the art in electronic stability systems and might also be beneficial to incorporate in a threat assessment for upcoming curves. We are therefore currently investigating a threat assessment algorithm based on this assumption.

CONCLUSIONS

It has been shown that the level of detail in the modelled vehicle dynamics has a significant impact on the maximum velocity profile for a vehicle negotiating a curve. The theoretically achievable velocity is however still very high and additional limitations of a driver's ability therefore need to be taken into consideration in order to achieve thresholds that have a higher practical benefit.

REFERENCES

[1] S. Ferguson, "The Effectiveness of Electronic Stability Control in Reducing Real World Crashes: A Literature Review", Traffic Injury Prevention, 8:4, 329-338, 2007

[2] W. Najm, B. Sen, J. Smith, B. Campbell, "Analysis of Light Vehicle Crashes and Pre-Crash Scenarios Based on the 2000 General Estimates System", Final Report, US Department of Transportation

[3] D. LeBlanc, J. Sayer, C. Winkler, R. Ervin, S. Bogard, J. Devonshire, M. Mefford, M. Hagan, Z. Bareket, R. Goodsell, T. Gordon, "Road Departure Crash Warning System Field Operational Test: Methodology and Results", Technical Report, University of Michigan Transportation Research Institute, 2006

[4] A. Eidehall, "Tracking and threat assessment for automotive collision avoidance ", Linköping University, PhD Thesis 1066, 2007

[5] Vägverket, "Vägar och gators utformning", Swedish Road Authority, Tech. Rep. 2004:80, 5 2004.

[6] E. Velenis, P. Tsiotras, "Optimal Velocity Generation for given Acceleration Limits; The Half-Car Model Case", Proceedings of the IEEE International Symposium on Industrial Electronics, 2005

[7] T.D. Gillespie, "Fundamentals of Vehicle Dynamics", Society of Automotive Engineers, 1992

[8] D.S. Naidu , "Optimal Control Systems", CRC Press, 2003

[9] M. Klomp, M Lidberg, "Safety Margin Estimation in Steady State Maneuvers", In Proceedings of the 8th International Symposium on Advanced Vehicle Control, 2006

[10] P. Falcone, F. Borrelli, J. Asgari, H. E. Tseng, D. Hvorat, "Predictive Active Steering Control for Autonomous Vehicle Systems", IEEE Transactions on control systems technology, 2007

[11] A. Van Zanten, "Bosch ESP Systems; 5 Years Of Experience", SAE, 2000

[12] H.E. Tseng, B. Ashrafi, D. Madau, T. Brown and D. Recker, "The Development of Vehicle Stability Control at Ford", IEEE/ASME Transactions on Mechatronics, vol 4, 1999

[13] H. Pacejka, "Tyre and Vehicle Dynamics", 2nd ed, Elsevier Ltd, 2006

[14] D. Casanova, "On Minimum Time Vehicle Manoeuvring: The Theoretical Optimal Lap", Ph.D Thesis, Cranfield University, 2000